Journal of Materials Chemistry

Cite this: *J. Mater. Chem.*, 2012, **22**, 16442

www.rsc.org/materials

PAPER

Transferability of solution processed epitaxial Ga:ZnO films; tailored for gas sensor and transparent conducting oxide applications

Moe Kevin, Wee Hong Tho and Ghim Wei Ho*

Received 25th April 2012, Accepted 21st June 2012
DOI: 10.1039/c2jm32590j

Problems associated with the costly production of Ga doped ZnO (Ga:ZnO) related to high-quality epitaxial films, which can only be grown on a lattice-matched single-crystal substrate using a vacuum system, have limited its wide-scale commercial applications. Moreover, for many practical applications, large-area devices must be fabricated on non-epitaxial glass, metal and other substrates. Here, we demonstrate a cost effective, low temperature aqueous synthesis, doping and transfer of high quality epitaxial Ga:ZnO on a non-epitaxial substrate. The capability of transferring epitaxial Ga:ZnO films may promote quick deployment of these high quality films for various electronic applications. We conclude the work with the demonstration of the Ga:ZnO films for gas sensing and dye-sensitized solar cell (DSSC) applications.

1. Introduction

Low temperature aqueous synthesis of ZnO has been actively pursued as a promising, attractive alternative to conventional means of semiconductor processing. The possibilities of doing away with costly vacuum systems and toxic precursors and the use of high temperatures will invariably change the way semiconductor devices can be fabricated and consumed. With a large direct bandgap (3.37 eV), high exciton binding energy (60 meV) and the ease of structural architecturing to suit various applications, ZnO is an ideal candidate for devices that demand transparent conductors, transparent thin film transistors (TFTs), optoelectronic devices such as lasers, solar photovoltaics and solid-state lighting as well as sensor devices for UV-visible photodetection and gas/liquid sensing.[1–8]

In the past few decades, solid-state based gas sensors have played an important role in chemical processes and environmental monitoring.[9] Among the various solid-state metal oxide sensors, semiconducting ZnO sensors have been widely investigated due to their chemically/thermally stable properties and sensitivity towards various harmful and combustible gases. Compared with bulk and thin film gas sensors, one-dimensional nanowire gas sensors are often fabricated to afford higher sensitivity due to large surface to volume ratio.[10] Using aqueous chemistry alone, a variety of ZnO nanostructures can be synthesized by simply changing precursors or using surfactants to alter growth dynamics.

In addition, aqueous synthesis also lends itself to the success of dopant incorporation, a process by which the electrical, optical or magnetic properties can be manipulated. Doping ZnO with group III (substituting Zn) or group VII (substituting O) elements is known to enhance n-type conductivity by increasing the electron concentration. The use of such dopants is central to the fabrication of transparent conducting oxides (TCOs). We have recently shown that textured single crystal Ga:ZnO films can be grown by a chemical route on a non-epitaxial substrate.[11] Novel, non-planar, transparent conducting electrodes consisting of pillars, cross-hatched trenches and pit structures were fabricated to produce films with increased surface roughness and enhanced light scattering capabilities essential for photovoltaic applications. To date, ZnO doped with Al, In or Ga and SnO_2 doped with In, Sb or F have been used as popular TCOs in the industry. These have been mainly deposited using vapour techniques such as pulsed laser deposition, chemical vapour deposition and RF magnetron sputtering.[12] However, the resulting films are typically polycrystalline. Acceptor states present at high angle grain boundaries give rise to depletion regions which extend into the interior of the grain. These regions form potential barriers which charge carriers have to overcome which in turn lowers both the free carrier concentration and the mobility, translating to higher resistivity. Therefore, high quality epitaxial films are especially suited as TCOs because they have fewer grain boundaries. However, problems associated with the costly production of Ga doped ZnO (Ga:ZnO) related to high-quality epitaxial films, which can only be grown on a lattice-matched single-crystal substrate using a vacuum system, have limited its wide-scale commercial applications. Moreover, for many practical applications, a large-area device must be fabricated on glass, metal and other substrates. For this reason, another processing step of separating or releasing the film from its epitaxial substrate is carried out. The most notable technique of releasing the film from its growth substrate is based on chemical etching of a

Department of Electrical and Computer Engineering, National University of Singapore, 4 Engineering Drive 3, 117576, Singapore. E-mail: elehgw@nus.edu.sg

sacrificial layer. However, the etching technique may have implications on its electrical and optical properties.

In this work, we demonstrate a cost-effective and low temperature method of devising large-scale epitaxial Ga:ZnO films on non-epitaxial substrates *via* an aqueous synthesis route and subsequent mechanical transfer. This work challenges the existing routes by which an epitaxial Ga:ZnO film can be made possible on a non-epitaxial substrate without resorting to high temperature, vacuum deposition and chemical etching processes and the excess consumption of expensive lattice matched substrates. The capability of transferring epitaxial Ga:ZnO films may promote quick deployment of these high quality films for various electronic applications. We conclude the work by presenting two proofs of concept of employing Ga:ZnO films for gas sensing and dye-sensitized solar cell (DSSC) applications.

2. Experimental details

2.1 Ga:ZnO film growth and transfer

Substrates were first sonicated in acetone and DI water for 5 min each. The seed solution was prepared using a 25 mM solution of $Zn(NO_3)_3$ in DI water in a 75 ml glass bottle, to which 0.6 g of ammonium nitrate was added and 1.10 mM of sodium tricitrate. The clean substrates $MgAl_2O_4$ spinel or c-Al_2O_3 sapphire were introduced into the seed solution and kept suspended upside down for 2 h. The seeded substrates were placed in a new bottle of solution containing 25 mM of $Zn(NO_3)_2$ and a varying amount of $Ga(NO_3)_3$. The pH of the solution was then adjusted to 10.88 using NH_4OH and kept at 85 °C for 4–6 h. Upon completion, the substrate was rinsed with IPA and dried at 50 °C.

The general processing steps are depicted in Fig. 1. First, a ZnO seed layer was grown epitaxially on a lattice matched substrate (Fig. 1a). The seed layer promoted nucleation and growth of a dense and continuous Ga:ZnO film (Fig. 1b and c). Then a receiver substrate was secured to the Ga:ZnO film using epoxy and mechanical lift off was carried out for film transfer (Fig. 1d and e). Using this method, the expensive spinel/sapphire substrate can be polished and reused after the transfer has been completed (Fig. 1f), thereby cutting down the consumption of expensive consumables.

2.2 Film characterization

SEM characterization was carried out using a JEOL FEG JSM 6700 F field-emission scanning electron microscope operating at 15 kV with a built-in energy dispersive X-ray (EDX) attachment

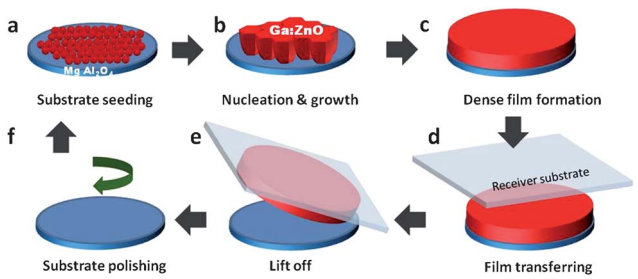

Fig. 1 Schematic diagrams of growth and transfer of a Ga:ZnO film from an epitaxial substrate to a receiver substrate.

(Oxford Instruments and Inca software). X-Ray photoelectron spectroscopy (XPS), VG ESCALAB MK2 equipped with an Mg Kα X-ray source, was employed to study the elemental composition of the doped films. X-Ray diffraction was carried out on a Philips X-ray diffractometer with Cu Kα radiation ($\lambda = 1.541$ Å). Transmission spectra were obtained using a Shimadzu UV-3600 UV-vis spectrophotometer with integrating sphere assembly. The Hall measurement was performed at room temperature by a Bio-Rad Hall system on a 1 cm by 1 cm sample using the Van der Pauw configuration. Indium was used to create an ohmic contact with the Ga:ZnO film.

2.3 Solar cell and gas sensing testing

Dye sensitized solar cells were fabricated using a Ga:ZnO film as the anode and counter-electrode. ZnO nanoparticles were 'doctor bladed' onto the Ga:ZnO film as a photoanode, and subsequently annealed at 300 °C for 30 min in a muffled furnace. The photoanode was then soaked in an ethanolic solution of N719 dye for 1 hour. For Pt counter-electrodes, 15 nm of Pt was sputtered using DC magnetron sputtering. The redox electrolyte was prepared with 0.1 M LiI, 0.05 M I_2, 0.6 M 1,2-dimethyl-3-propylimidazolium iodide, and 0.5 M 4-*tert*-butylpyridine in acetonitrile. All devices were tested under AM1.5 conditions using a Newport 91160A solar simulator. The light source comprised a 150 W Xe lamp and the light intensity corresponded to AM1.5 (100 mW cm^{-2}) calibrated with a standard Si cell (Oriel SRC1000 TC).

Gas sensors were fabricated based on ZnO nanorods grown on the Ga:ZnO film and were tested at various concentrations of ethanol. The ethanol and clean dry air (CDA) were supplied to the setup *via* mass flow controllers. The gas sensor was placed in the sensing chamber and electrical leads from the sample were connected to a sourcemeter (Keithley 4200-SCS) *via* an electrical feed-through.

3. Discussion and results

Reports by Lange and co-workers on seed layer synthesis described the abrupt change in pH of the seed solution to achieve sufficient thermodynamic driving force to effect the nucleation of ZnO on the spinel surface.[13] Time evolution crystal growth was investigated, where Fig. 2 shows the Volmer–Weber growth of the seed layer morphology over a time span of 100 min on spinel. Nucleation could be observed as early as 10 min after immersion. At 25 min, the surface was covered with an even distribution of distinctively hexagonal ZnO crystals (Fig. 2a). Crystal sizes ranged from 200–900 nm. At 50 min and 75 min, coalescence of the films became increasingly evident as the hexagonal crystals join up to form irregularly shaped islands while maintaining their individual sizes (Fig. 2b and c). This suggests that complete coalescence observed at 100 min (Fig. 2d) is brought about by an increase in the crystal number density, rather than an increase in the individual crystal size itself. It is well established that ZnO crystals grown by an aqueous chemical route express preferential growth along the *c* direction. From Fig. 2b and c, one observes that the planes belonging to the $\{10\bar{1}0\}$ family are all parallel, suggesting that high angle grain boundaries do not exist upon coalescence. The final seed layer thickness after 100 min was

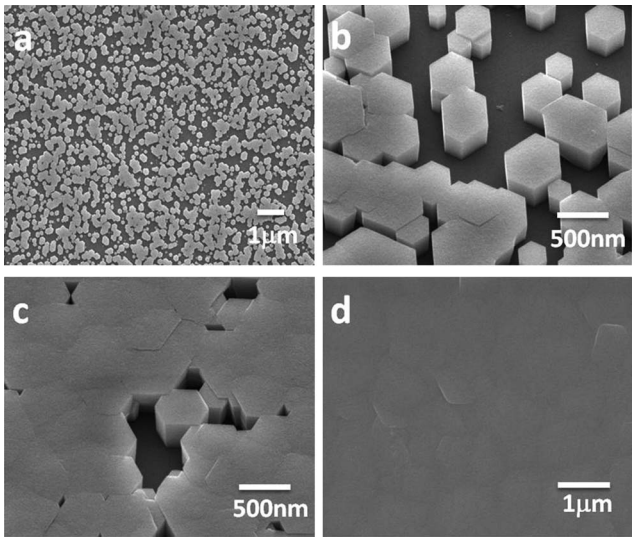

Fig. 2 SEM images of the nucleation and growth of Ga:ZnO films at different growth durations of (a) 25, (b) 50, (c) 75 and (d) 100 minutes.

approximately 400 nm. Another important feature of the film growth is the low aspect ratio (~0.8) of the crystals which demonstrates the effect of citrate anions as a surfactant. An increasing concentration of citrate gives rise to well-defined hexagonal crystals of increasing diameters. In principle, the diameter of the crystals can be controlled by tuning the concentration of citrate ions which in turn control the film thickness. The citrate anions function as growth inhibitors by selectively adhering to the positively charged Zn terminated plane, retarding the *c*-direction growth rate relative to the lateral *a*-direction. This allows the crystal to grow faster in the *a* direction,[14] thereby facilitating coalescence.

Ga:ZnO films were then grown on the coalesced seed layer. Fig. 3 shows the top and cross-sectional views of Ga:ZnO films grown using 0, 1.5 and 3.0 mM of $Ga(NO_3)_3$ dopant. With 0 and 1.5 mM of dopant (Fig. 3a and d) the resulting films were smooth and well-coalesced. However, at the higher dopant concentration of 3.0 mM, numerous pits and caverns were found consistently throughout the otherwise smooth film (Fig. 3e). Cross-sectional SEM revealed that these pits originated from the Ga:ZnO layer, and not from the seed (Fig. 3f). This has been attributed to the presence of competing dopant species which inhibit the growth of the film.[15]

XRD was performed on the films grown with 0, 1.5 and 3.0 mM of $Ga(NO_3)_3$ on spinel as shown in Fig. 4a. XRD is an effective way of detecting the presence of secondary phases such as Ga_2O_3 and $ZnGa_2O_4$ where the Ga^{3+} ion located at the grain boundary region can result in the formation of a secondary phase within the Ga:ZnO thin film. Diffraction peaks corresponding to secondary phases are absent whilst the dominant diffraction peak observed at 2θ ~34° in all samples arises from the ZnO (0002) plane. This indicates that all the films were of pure ZnO phase, highly *c*-axis oriented with characteristic of the hexagonal ZnO wurtzite film. The lowest surface energy of the (0002) plane as compared to other ZnO planes has led to its fast growth. At 3.0 mM, XRD showed the presence of the (101) peak belonging to ZnO. We believe that this is due to the pitted morphology as shown in the SEM images of Fig. 3e and f. Irregularities in the film structure could be due to heterogeneous growth of ZnO nuclei which do not adhere to the bulk orientation. By keeping the dopant concentration at 1.5 mM, the crystallinity and film

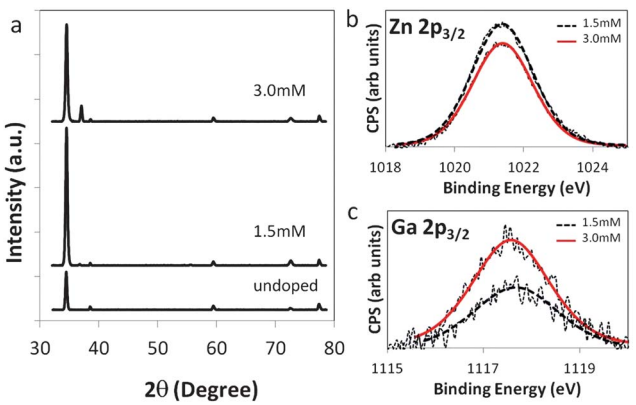

Fig. 4 (a) XRD and XPS spectra of (b) Zn 2p and (c) Ga 2p of various doping concentrations.

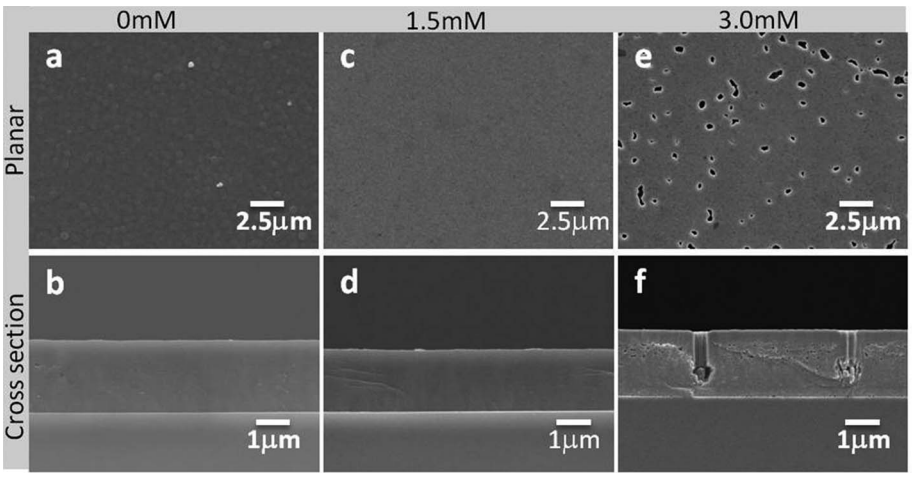

Fig. 3 SEM images of planar and cross-sectional views of Ga:ZnO films grown at different dopant concentrations.

Table 1 Summary of electrical properties of doped and undoped films

Sample	Sheet resistance (Ω sq^{-1})	n (cm^{-3})	Mobility (cm^{-2} V^{-1} s^{-1})	Ga/(Ga + Zn)
Undoped	1100	5.5×10^{18}	20.70	0
1.5 mM $Ga(NO_3)_3$	6.73	8.2×10^{19}	41.50	0.07
3.0 mM $Ga(NO_3)_3$	26.9	7.5×10^{19}	11.40	0.15

integrity were maintained. Fig. 4b and c show high-resolution XPS spectra of Zn 2p and Ga 2p obtained from Ga:ZnO films grown with 1.5 and 3 mM of $Ga(NO_3)_3$ dopant. The change of chemical state in the Ga:ZnO films grown with different doping concentrations was studied. By fitting the peaks Ga $3p_{3/2}$ (1117.65 eV) and Zn $3p_{3/2}$ (1021.40 eV), Ga/(Ga + Zn) fractions for 1.5 mM and 3.0 mM doped samples were calculated to be 0.07 and 0.15 respectively. Within the range of dopant concentrations used, Ga incorporation increased approximately linearly with the concentration of $Ga(NO_3)_3$ used during the growth.

Samples of 1 × 1 cm were used for Hall measurements using the Van der Pauw configuration with 100 nm of evaporated Al as the contacts. The results are summarized in Table 1. Undoped ZnO exhibited n-type behavior with an $n = 5.5 \times 10^{18}$ cm^{-3}. The intrinsic n-type conductivity in ZnO is caused by H incorporation present in high pH growth, as well as intrinsic defects such as O vacancies and Zn interstitials.[16] On the other hand, both 1.5 mM and 3.0 mM doped samples showed $n = 8.2 \times 10^{19}$ cm^{-3} and $n = 7.5 \times 10^{19}$ cm^{-3}, respectively. The small difference in carrier concentration between the doped samples indicates that the 3.0 mM sample had approximately the same number of Ga_{Zn}, which contribute one free electron each. The excess Ga for the 3.0 mM sample occupies electrically inactive sites which function as impurity scatterers. This is further supported by the relatively lower mobility of the 3.0 mM doped sample. Films doped with 1.5 mM of $Ga(NO_3)_3$ exhibited the best conductivity with an average sheet resistance of 6.73 ohm sq^{-1}. Electron transport in lightly doped Ga:ZnO ($n < 10^{20}$ cm^{-3}) is known to be grain boundary limited, while in highly doped samples, electrons are able to tunnel through energy barriers at the grain interface.[17] Our samples demonstrated that superior sheet resistances could still be obtained despite the relatively lower carrier concentrations (~8×10^{19} cm^{-3}) because high angle grain boundaries and the associated scattering mechanisms are significantly minimized in epitaxial films.

After synthesis, the Ga:ZnO film was mechanically lifted off the original growth substrate and transferred onto a receiver substrate *e.g.* glass. Subsequently, the spinel/sapphire substrate was polished and reused. Hence, technical challenges of obtaining high-quality epitaxial Ga:ZnO film on non-epitaxial and cheap substrates can be overcome by the ability of film transfer. The issue of using an expensive lattice matched epitaxial substrate is not of concern since it is mechanically polished and reused for the next growth. Furthermore, it is shown that an entire piece of the Ga:ZnO film can be effectively transferred. Currently, the size of our transferred Ga:ZnO film is limited only by the size of the original epitaxial substrate. In this case, we have utilized a 2 inch diameter spinel substrate for the growth of epitaxial Ga:ZnO film which is then transferred to a glass substrate as shown in Fig. 5a. The transferred film exhibits good optical transmission (Fig. 5a). For comparison, Fig. 5b shows the transmissivity of the transferred Ga:ZnO films in comparison with commercial ITO and FTO. It is important to note that the transmission spectra for transferred Ga:ZnO includes the epoxy layer. Even so, it is evident that the transferred Ga:ZnO is comparable in terms of optical transmission with the commercial substrates. Disparities in transmission within the UV range are attributed to the difference in bandgaps between ZnO and SnO_2 and Moss–Burstein shifts.

Fig. 5c shows a cross-sectional SEM image of a Ga:ZnO film that has been transferred to a glass substrate; Fig. 5d shows the

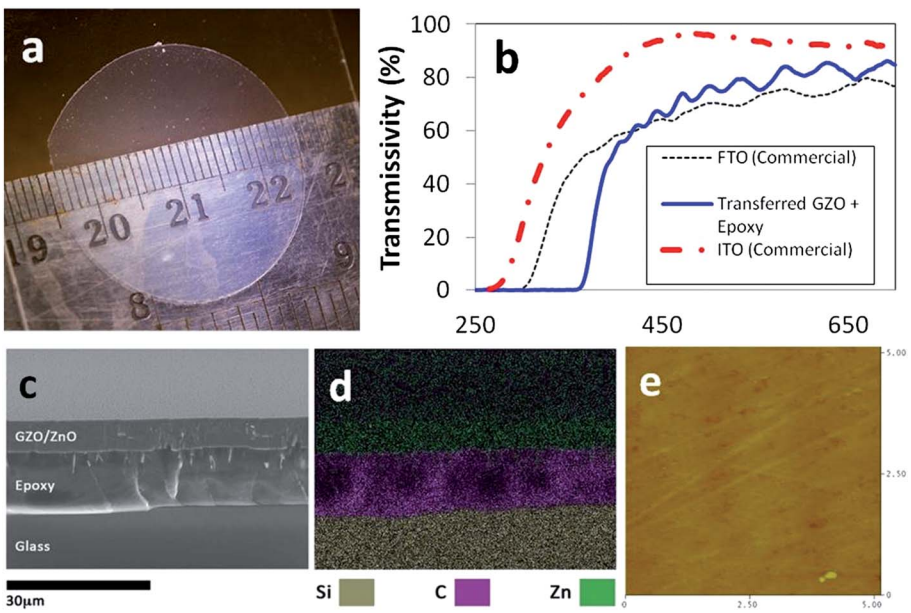

Fig. 5 (a) Digital photograph of transferred Ga:ZnO film on glass. (b) Transmission spectra of Ga:ZnO film and other commercial transparent conductors. (c) SEM image of transferred Ga:ZnO film and (d) its corresponding EDX elemental map. (e) AFM image (5 × 5 μm) of the Ga:ZnO film.

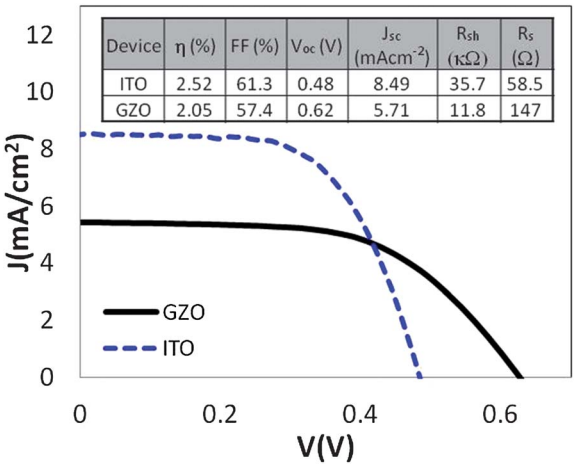

Fig. 6 *J–V* curves and cell characteristics of Ga:ZnO and ITO transparent conductor DSSCs.

corresponding spatially resolved EDX map, clearly showing the film, epoxy and glass layers. After the transfer process, SEM images revealed that the surfaces of the transferred films were smooth, and macroscopic defects such as cracks were not present. Fig. 5e shows a AFM scan (5 × 5 μm) of a film grown with 1.5 mM $Ga(NO_3)_3$. The scan shows a smooth, fully coalesced surface with a rms roughness of ~5.1 nm. Smooth films are essential for producing highly transparent conductors as surface irregularities serve to scatter light. In addition, resistivity measurements showed that electrical properties of the films remained invariant after the transfer, making such films suitable for optoelectronic applications that demand optical transmissivity and high conductivity.

A DSSC and a gas sensor were fabricated to demonstrate the application of the transferred Ga:ZnO. DSSC photoanodes were fabricated by "doctor blading" ZnO nanoparticle films on transferred Ga:ZnO films and commercial ITO. Fig. 6 shows the current–voltage characteristics of a DSSC fabricated on a transferred Ga:ZnO film on glass and commercial ITO with power conversion efficiencies of 2.05% and 2.52% as well as fill factors of 57.4% and 61.3%, respectively. Unlike other material's systems used in DSSCs, the photoanode ZnO nanoparticles and the transparent conductor Ga:ZnO film belong to the same material system. The advantage of using a ZnO photoanode on Ga:ZnO is that the band at the homojunction (neglecting trap states) bends in the direction of the electron injection from the photoanode to the Ga:ZnO transparent conductor. The band alignment which results in a built-in electric field which promotes the electron injection from the ZnO nanoparticles into the Ga:ZnO films.

As for the gas sensing application, two isolated blocks of Ga:ZnO contact pads (Fig. 7a) were initially fabricated using a conventional photolithography process.[10] Subsequently, ZnO nanorods were synthesized to bridge the Ga:ZnO contact pads to form a closed electrical loop as shown in the (top view) SEM image of Fig. 7b. The nanorods were synthesized by spin coating ZnO colloids onto the Ga:ZnO contact pads and undergo hydrothermal growth at 90 °C for 2 hours.[18] The electrical connectivity and gas sensing measurements were obtained as shown schematically in Fig. 7c. Such a configuration was chosen because of the comparatively higher surface area that nanorods possess as compared to films. Fig. 7d shows current–time measurement of the ZnO sensor with various ethanol vapor concentrations. The resistance of the gas sensor is observed to decrease in ethanol ambient and increase in air ambient, indicating n-type behavior. It is known that oxygen molecules tend to adsorb onto a ZnO nanowire surface as physisorbed oxygen which extracts and localizes electrons from the conduction band at the oxygen vacancy site to form chemisorbed oxygen species, O_2^-, O^- and O^{2-}. At room temperature, O_2^- is favorably chemisorbed and functions as an acceptor resulting in the

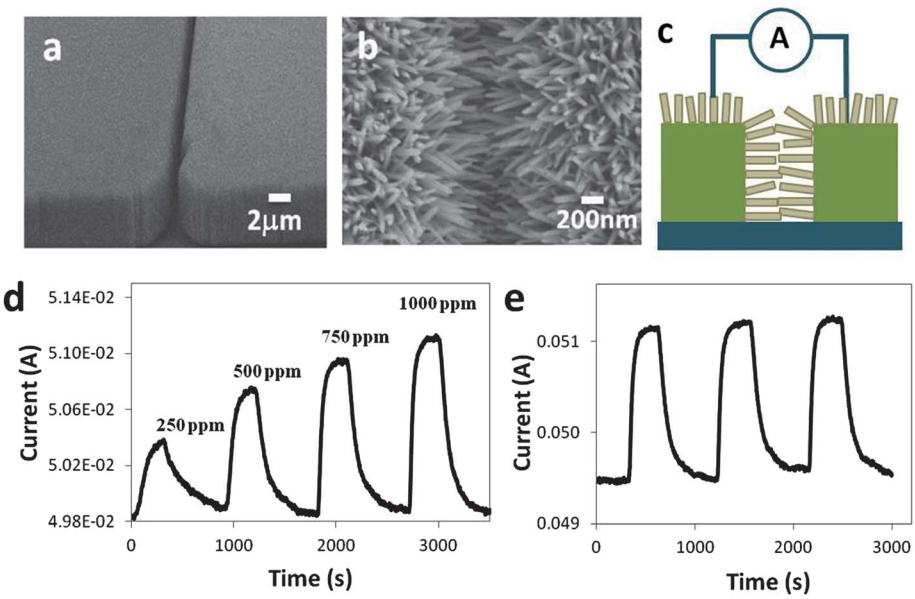

Fig. 7 SEM image of (a) Ga:ZnO contact pads before the growth of nanorods, (b) top view of ZnO nanorods grown from spin coated colloids on Ga:ZnO contact pads and (c) schematic of the constructed gas sensor based on bridging ZnO nanorods. (d) Ethanol sensing at various vapor concentrations. (e) Cycling of ethanol sensing at 250 ppm.

"de-activation" of donors leading to a decrease in conductivity or electron-depleted space charge region at the surface of the nanorods.[19] When ZnO nanorods are exposed to ethanol vapor, the chemisorbed oxygen ions are reduced to release electrons to the conduction band of the ZnO nanowire surface as depicted in eqn (1):

$$C_2H_5OH\ (gas) + O_2^- \leftrightarrow CH_3CHO + H_2O + e^- \quad (1)$$

The reaction initiates oxidation of ethanol by dehydrogenation to form the CH_3CHO (acetaldehyde) intermediate, which may eventually reduce to CO_2 and H_2O.[19] This leads to the "re-activation" of the donor sites and an increase in the conductance of the nanorods. The sensor performance is quantified based on the gas response which is defined as $(R_{eth} - R_{CDA})/R_{eth} \times 100\%$, where R_{eth} and R_{CDA} are the resistances of the device in ethanol vapor and CDA, respectively. For ethanol vapor of 250, 500, 750, and 1000 ppm, the responses are 1.10, 1.69, 2.20, and 2.43%, respectively. Thus, it is noted that only a few relatively short nanorods bridged between the Ga:ZnO contact pads may have contributed to the relatively low responses.[20] The fabricated sensor exhibits highly consistent responses over few cycles, which translates to device stability (Fig. 7e).

4. Conclusion

Epitaxial Ga:ZnO films were synthesized on both $MgAl_2O_4$ and c-Al_2O_3 single crystal substrates using a low temperature aqueous procedure. The films were characterized to confirm the presence of incorporated Ga ions which was accompanied by an improvement in conductivity. Effective lift-off to transfer the Ga:ZnO film from its epitaxial substrate to a non-epitaxial substrate is made possible without resorting to high temperature, vacuum deposition and chemical etching processes and the excess consumption of expensive lattice matched substrates. Finally, we have demonstrated a comparable power conversion efficiency of the transferred Ga:ZnO film to the commercial ITO solar cell. Furthermore, the Ga:ZnO film with ZnO nanorods is shown to be a stable ethanol vapor sensor.

Acknowledgements

This work is supported by the National University of Singapore (NUS) grant R-263-000-532-112 and R-263-000-653-731. The authors would like to thank Gah Hung Lee for his valuable work on X-ray photoelectron spectroscopy.

References

1 A. B. Djurišić, X. Chen, Y. H. Leung and A. M. C. Ng, *J. Mater. Chem.*, 2012, **22**, 6526–6535.
2 S. H. Ko, D. Lee, H. W. Kang, K. H. Nam, J. Y. Yeo, S. J. Hong, C. P. Grigoropoulos and H. J. Sung, *Nano Lett.*, 2011, **11**, 666–671.
3 X. W. Sun, J. Z. Huang, J. X. Wang and Z. Xu, *Nano Lett.*, 2008, **8**, 1219–1223.
4 B. Liu, Z. Wang, Y. Dong, Y. Zhu, Y. Gong, S. Ran, Z. Liu, J. Xu, Z. Xie, D. Chen and G. Shen, *J. Mater. Chem.*, 2012, **22**, 9379–9384.
5 H. H. Guo, Z. H. Lin, Z. F. Feng, L. L. Lin and J. Z. Zhou, *J. Phys. Chem. C*, 2009, **113**, 12546–12550.
6 S. Jeong and J. Moon, *J. Mater. Chem.*, 2012, **22**, 1243–1250.
7 L. Wang, Z. Lou, T. Fei and T. Zhang, *J. Mater. Chem.*, 2012, **22**, 4767–4771.
8 Z. H. Lim, Z. X. Chia, M. Kevin, A. S. W. Wong and G. W. Ho, *Sens. Actuators, B*, 2010, **151**, 121–126.
9 P. T. Moseley, *Meas. Sci. Technol.*, 1997, **8**, 223–237.
10 W. L. Ong, C. Zhang and G. W. Ho, *Nanoscale*, 2011, **5**, 4206–4214.
11 M. Kevin, G. H. Lee and G. W. Ho, *Energy Environ. Sci.*, 2012, **5**, 7196–7202.
12 K. Ellmer, A. Klein and B. Rech, *Transparent Conductive Zinc Oxide: Basics and Applications in Thin Film Solar Cells, Springer Series in Materials Science*, 2008.
13 J. J. Richardson and F. F. Lange, *Cryst. Growth Des.*, 2009, **9**, 2570–2581.
14 Z. R. Tian, J. A. Voigt, J. Liu, B. Mckenzie, M. J. Mcdermott, M. A. Rodriguez, H. Konishi and H. Xu, *Nat. Mater.*, 2003, **2**, 821–826.
15 H. Q. Le, S. K. Lim, G. K. L. Goh, S. J. Chua and J. X. Ong, *J. Electrochem. Soc.*, 2010, **157**, H796–H800.
16 C. F. Windisch, Jr, G. J. Exarhos, C. Yao and L. Q. Wang, *J. Appl. Phys.*, 2007, **101**, 123711.
17 K. Ellmer, *J. Phys. D: Appl. Phys.*, 2001, **34**, 3097–3108.
18 M. Kevin, Y. H. Fou, A. S. W. Wong and G. W. Ho, *Nanotechnology*, 2010, **21**, 315602–315610.
19 S. Matsushima, T. Maekawa, J. Tamaki, N. Miura and N. Yamazoe, *Chem. Lett.*, 1989, **18**, 845–848.
20 H. N. Hieu, N. M. Vuong, H. Jung, D. M. Jang, D. Kim, H. Kim and S.-K. Hong, *J. Mater. Chem.*, 2012, **22**, 1127–1134.